Journal of Material Cycles and Waste Management (2018) 20:1499–1506
https://doi.org/10.1007/s10163-018-0710-0

ORIGINAL ARTICLE

Study on desulfurization performance of MnO_2-based activated carbon from waste coconut shell for diesel emissions control

Xuecheng Liu[1,2] · Lin Liu[1] · Yugo Osaka[3] · Hongyu Huang[1] · Zhaohong He[1] · Yu Bai[1] · Shijie Li[1] · Jun Li[4] · Huhetaoli[1]

Received: 5 June 2017 / Accepted: 29 January 2018 / Published online: 8 February 2018

Abstract

Increasing concern about the air pollution caused by sulfur dioxide (SO_2) from diesel exhaust has resulted in the improvement of low-temperature desulfurization materials for the combined SO_2 trap. In this study, coconut shell activated carbon (AC) is pretreated by nitric acid to prepare MnO_2-based activated carbon materials for SO_2 removal. The prepared materials are characterized intensively by SEM, TEM, BET, XRD, FTIR, and XPS. The SO_2 capture capacity of these materials are measured at low temperature by thermogravimetry, and the SO_2 equilibrium adsorption characteristic is also investigated. The results show that the concentrations of nitric acid do not significantly change the textural properties of MnO_2-based AC materials. The content of surface-oxygenated groups (carbonyl carbon and transition) initially increases with the HNO_3 concentration rising and reaches the maximum value when the HNO_3 concentration is 10 mol/L, resulting in the enhancement of the SO_2 capture capacity. SO_2 capture capacity of MnO_2-based activated carbon decreases after regeneration and keeps stable after several cycles of thermal regeneration. The experimental data for SO_2 adsorption on MnO_2-based AC composite can fit the Freundlich model well in comparison with Langmuir model.

Keywords SO_2 · MnO_2 · Activated carbon · Nitric acid · Freundlich model

Introduction

Sulfur dioxide (SO_2) from diesel engine exhaust is a serious threat to the environment and human health, because SO_2 has the major role in generating acid rain and deactivating the NO_x removal catalysts [1–3]. Many technologies have been proposed to remove SO_2 from diesel engine exhaust. Among these, the compact SO_2 trap device upstream of NO_x conversion device has been used successfully for the removal of SO_2 to improve the longevity of NO_x removal catalysts against SO_2 poisoning [4–6].

As the temperature of diesel engine exhaust is in a wide region from 50 to 650 °C, a combined SO_2 trap is proposed to completely capture the SO_2 in this temperature region [7]. The combined SO_2 trap has three parts: high temperature materials, middle temperature materials and low-temperature materials. The desulfurization material is an important factor for designing the combined SO_2 trap device. The carbonates exhibits good reactivity with SO_2 at the reaction temperature range from 400 to 650 °C, and the desulfurization rate declines below 400 °C for the reason that the reaction activity is limited by decarbonation [8]. Metal oxides (such as MgO [9], V_2O_5 [10] and hydrotalcite-like compounds [11]) with sulfate reaction path $\left(M_xO_y + ySO_2 + 0.5yO_2 \rightarrow M_x(SO_4)_y\right)$ have good SO_2 capture performance over the temperature range from 200 to 450 °C. Based on these fundamental studies, it has been found that most desulfurization materials are focused on the desulfurization performance from 200 to 650 °C for SO_2

✉ Hongyu Huang
huanghy@ms.giec.ac.cn

✉ Zhaohong He
hezh@ms.giec.ac.cn

1 Key Laboratory of Renewable Energy, Guangzhou Institute of Energy Conversion, Chinese Academy of Sciences, No. 2 Nengyuan Rd. Wushan, Tianhe District, Guangzhou 510640, People's Republic of China

2 Chongqing Key Laboratory of Catalysis and Functional Organic Molecules, College of Environmental and Biological Engineering, Chongqing Technology and Business University, Chongqing 400067, China

3 Kanazawa University, Kakuma, Kanazawa, Ishikawa 920-1192, Japan

4 Nagoya University, Furo-cho, Chikusa-ku, Nagoya 464-8603, Japan

traps, and limited studies on the desulfurization performance from 50 to 200 °C desulfurization materials for the combined SO_2 trap have been reported.

For developing the desulfurization performance of the combined SO_2 trap, the improvement of low-temperature desulfurization activity of materials for the combined SO_2 trap is needed. Rubio [12] investigated the SO_2 capture performance of coal fly ash based on carbon materials at flue gas desulfurization conditions. Tseng [13] studied the desulfurization activity of copper oxide (CuO) supported on activated carbon over the low-temperature range. In the previous studies [14, 15], MnO_2 has been found to exhibit remarkable sulfur dioxide capture capacity. MnO_2 supported on AC have a promising prospect used as low-temperature desulfurization materials for the combined SO_2 trap [7]. Manganese supported on activated carbon treated by HNO_3 exhibited high SO_2 removal capacity [16]. However, the relationship between the amount of surface-oxygenated groups and SO_2 removal capacity of MnO_2-based AC has not been reported yet.

In the present work, the high-specific-surface-area coconut shell AC is pretreated by nitric acid to modify the surface functional groups and used as a support to prepare MnO_2-based AC composite by situ deposition method. Effects of the surface-oxygenated groups of MnO_2-based AC composite by nitric acid treatment on the SO_2 capture capacity are studied. The SO_2 adsorption characteristics and regeneration performance of MnO_2-based activated carbon composite at low-temperature range are also investigated.

Experimental section

Materials

The activated carbon (BET surface area of 1250 m^2/g) made from waste coconut shells was supplied by Xinsen Chemical Industry Co. Ltd. Potassium permanganate and manganese acetate tetrahydrate were purchased from Beijing Chemical Co., Ltd., People's Republic of China and were of analytical reagent grade.

The MnO_2-based AC composites were prepared by situ deposition method, the formation procedures as shown in Fig. 1. The activated carbon was pretreated with different concentrations of HNO_3 (from 0 to 15 mol/L) at 80 °C for 6 h, then washed with a lot of distilled water, and dried in a vacuum at 110 °C overnight. 2 g pretreated AC was added to 0.03 mol/L 100 mL $KMnO_4$ solution and stirred at room temperature condition for 2 h, then gradually added 0.045 mol/L 100 ml $Mn(CH_3COO)_2$ solution and stirred at room temperature condition for 5 h, then washed with a lot of distilled water, and eventually dried in air dry oven at 110 °C overnight. The product is denoted as MnO_2–ACx, where x represents the concentration of HNO_3.

Characterization

In this study, the textural properties of the samples were analyzed by N_2 adsorption–desorption isotherms using Micromeritics ASAP 2020 apparatus. The specific surface area of these samples was measured by the Brunauer–Emmett–Teller (BET) with the nitrogen adsorption uptake at the boiling point of nitrogen of 77 K using a capacitive measurement method. The pore volumes were measured by nitrogen physisorption under normal relative pressure of 0.1–1.0 using the Barrett–Joyner–Halenda (BJH) method. Surface observation of the samples was conducted by scanning electron microscopy (SEM, Hitachi S-4800). Before SEM experiment, the sample was pretreated by gold-sputtering. Transmission electron microscopy (TEM) images were recorded on a JEOL JEM-2100F electron microscope. The powder sample was ultrasonically dispersed in acetone for 30 min at room temperature and dipped onto a carbon-coated copper grid. The crystal structures were further determined by X-ray diffraction (XRD, X'Pert Pro MPD, Cu Kα radiation). Fourier transform infrared (FTIR) spectra were recorded using a Tensor 27 spectrometer with KBr pellet method. X-ray photoelectron spectroscopy (XPS) was conducted to determine the chemical composition and functional groups using an XSAM-800 spectrometer (Kratos, UK) with Al (1486.6 eV) under ultrahigh vacuum (UHV) at 12 kV and 15 mA. Energy calibration was performed by recording the core level spectra of Au $4f_{7/2}$ (84.0 eV) and Ag $3d_{5/2}$ (368.30 eV).

SEM and TEM analyses are employed to visualize the morphology and structure of AC and MnO_2–AC10, as shown in Fig. 2. It can be seen that AC is a planar architecture with a well-defined pores (Fig. 2a). This planar-architecture structure of AC facilitates the adsorption of reagents and exposes more active sites for SO_2 removal. After deposition, a large number of nano-flake MnO_2 particles are only formed and highly dispersed on the surface

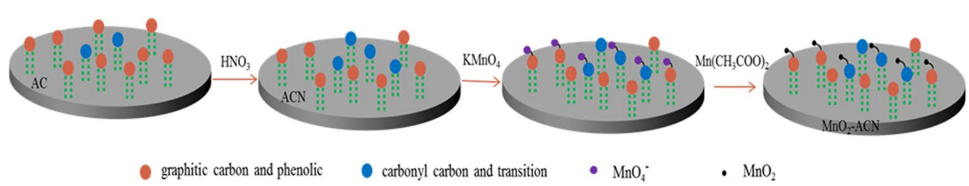

Fig. 1 Illustration of the formation procedures of MnO_2-based AC composite

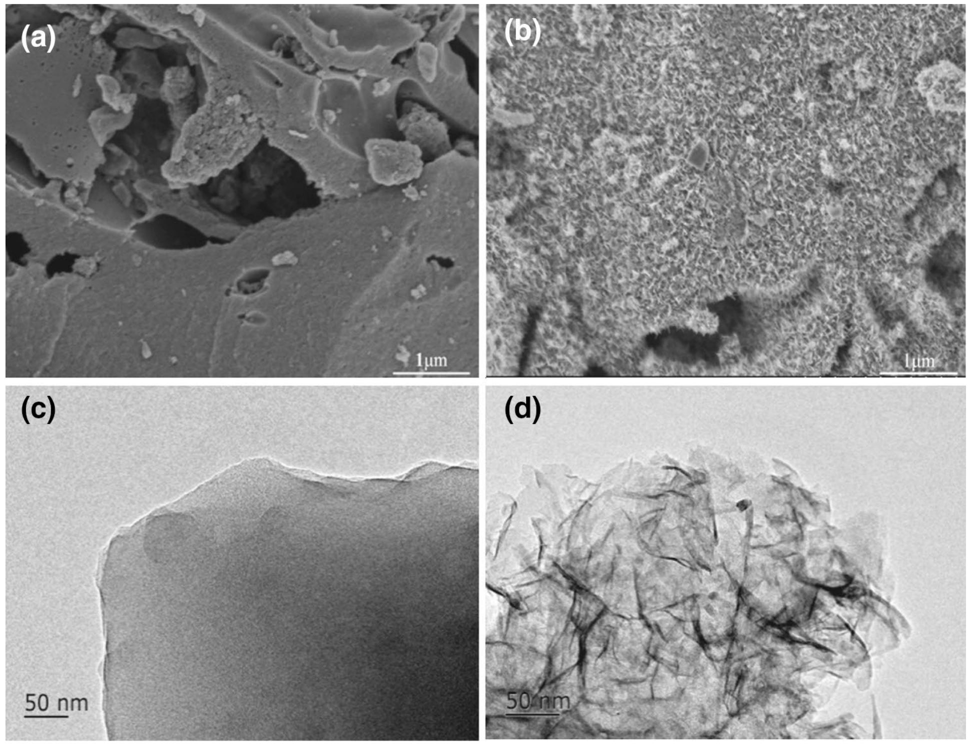

Fig. 2 SEM and TEM images of AC (**a, c**) and MnO_2–AC (**b, d**)

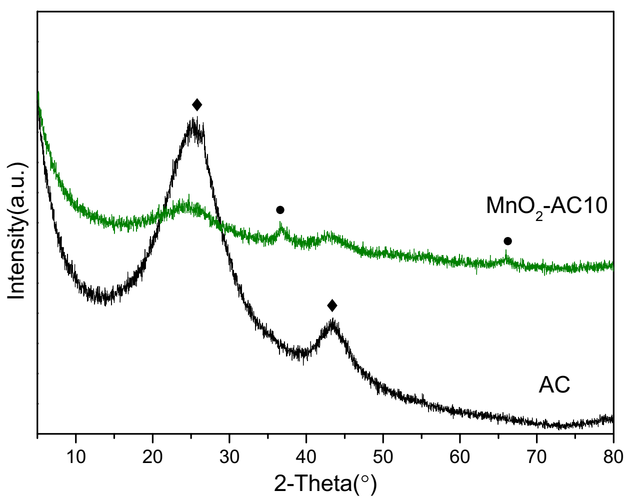

Fig. 3 XRD patterns of AC and MnO_2–AC10 (filled circle) reflections of MnO_2 (filled diamond) reflections of carbon

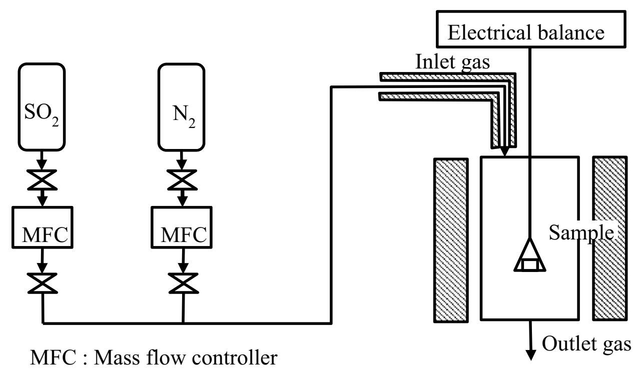

Fig. 4 Schematic drawing of TG analysis

of AC and no free nanoparticles are formed outside the AC nanosheets (Fig. 2b, d). The MnO_2 nanoparticles are confirmed by XRD analysis (Fig. 3). The diffraction peaks of as-prepared MnO_2–AC10 are similar to those of hexagonal MnO_2 (JCPDS 30-0820) and the reflection peaks of layered AC become much lower, which also indicating that nano-flake MnO_2 particles are homogeneously formed on the AC surface.

Desulfurization performance evaluation

Thermogravimetry (TG) was used in this study to measure the SO_2 capture performance of the prepared materials. Figure 4 shows a schematic drawing of the TG analysis experiment. The amount 50 mg of a sample on a quartz crucible was slowly (5 K/min) heated to the target temperature in the atmosphere of nitrogen, and maintained this condition for about 2 h. Reactant gas flow (500 ppm SO_2 in base N_2) was controlled by mass flow controller. The total flow gas rate was 2 Ls/min. The reaction temperature of the TG experiment ranged from 50 to 200 °C for 40 min. The used MnO_2–AC were regenerated in N_2 atmosphere at a flow rate of 500 mL/min and at 360 °C for 1 h. Then the regenerated sample was cooled to reaction temperature under pure N_2 steam. After that, a 2 Ls/min gas mixture (500 ppm SO_2 in base N_2) was controlled by mass flow controller and added into the reactor for further desulfurization–regeneration testing.

The SO_2 capture performance of samples was measured. The SO_2 capture performance per unit mass P is expressed by the following equation:

$$P = \frac{s_t - s_0}{s_0} \left[g_{SO_2}/g_{Material}\right] \quad (1)$$

where P is the SO_2 capture performance per unit mass [$g_{SO2}/g_{Material}$], s_0 is the initial weight [mg], and s_t is the weight after t seconds [mg].

Results and discussion

SO_2 capture performance of the prepared materials

The SO_2 capture performance of the prepared MnO_2-based activated carbon composites (MnO_2–AC0, MnO_2–AC5, MnO_2–AC10 and MnO_2–AC15) was measured at the following conditions: 100 °C and 500 ppm SO_2 in base N_2 for 40 min. Figure 5 shows the SO_2 capture capacity of the prepared materials. The SO_2 capture performance of MnO_2–AC0 was 26 mg/g. The SO_2 capture performance of MnO_2-based activated carbon composite increased after nitric acid pretreatment. When the acid concentration is below 10 mol/L, the SO_2 capture capacity has improved with the increase of treatment concentration, and the SO_2 capture capacity has attained the highest as the treatment concentration is 10 mol/L. The SO_2 capture capacity of MnO_2–AC10 is 44 mg/g, which is significantly higher than the low-temperature desulfurization material, such as coal fly ash (13 mg/g) [12] and CuO/AC (below 10 mg/g) [13]. However, when the pretreatment concentration is above 10 mol/L, the SO_2 capture capacity has reduced with the increase of treatment concentration. The SO_2 capture capacity of MnO_2–AC15 has decreased to 28 mg/g. It is reported that the content of the surface-oxygenated groups of activated carbon increases with the increase of the acid treatment concentration [17], and the surface functional groups are the important factors for the SO_2 removal [16].

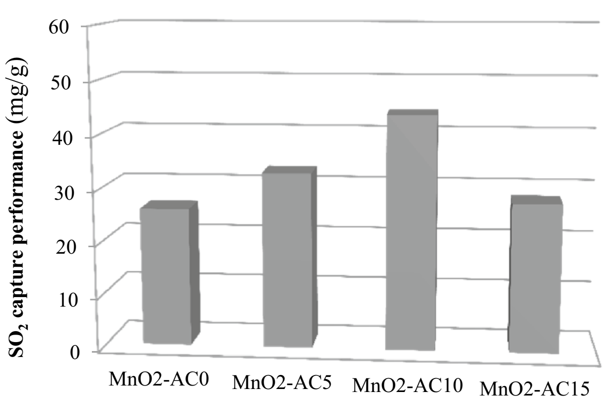

Fig. 5 SO_2 capture performance of the prepared samples (experimental conditions: 100 °C, 500 ppm SO_2 in base N_2)

Textural characteristic analysis of MnO_2-based AC materials

The textual properties of the prepared MnO_2-based activated carbon are characterized by N_2 adsorption–desorption instruments apparatus and are shown in Table 1. The BET surface area and pore volume of the MnO_2–AC0 are 1012 m^2/g and 0.17 cm^3/g, respectively. After pretreated by HNO_3, the pore volume and average pore diameter of MnO_2-based activated carbon are in the range of 0.17–0.20 cm^3/g and 3.12–3.15 nm, respectively. It has been reported in many works that the liquid phase oxidation by HNO_3 may not significantly change the textural properties of AC [18, 19]. The BET surface areas of the MnO_2-based activated carbon are slightly reduced from 1012 to 918 m^2/g after nitric acid treatment. The slight decrease in the surface area of MnO_2-based AC may be due to the abundant presence of oxygenated groups introduced on the surface of the AC by the pretreatment with HNO_3, which possibly block the entry of N_2 inside the small pores [17, 20].

Surface functional groups on MnO_2-based AC samples

The FTIR was carried out to determine the functional groups on the prepared MnO_2-based activated carbon composites. The FTIR spectrum of the prepared materials (MnO_2–AC0,

Table 1 Textural properties of MnO_2-based AC materials

Samples	Treated concentration of HNO_3 (mol/L)	BET surface area (m^2/g)	Pore volume (cm^3/g)	Average pore diameter (nm)
MnO_2–AC0	0	1012	0.17	3.13
MnO_2–AC5	5	992	0.17	3.12
MnO_2–AC10	10	971	0.20	3.13
MnO_2–AC15	15	918	0.19	3.15

MnO_2–AC5, MnO_2–AC10, and MnO_2–AC15) is illustrated in Fig. 6. From the FTIR spectrum of the prepared materials shown in Fig. 6, the peaks around 3430 cm^{-1} should be attributed to the O–H stretching vibration [21], and the bands around 1623 cm^{-1} are normally attributed to O–H-bending vibrations combined with Mn atoms [22]. The relatively sharp peaks around 1395 cm^{-1} should be ascribed to C=O stretch from carboxylic groups [23]. The C=O stretch peaks of MnO_2–AC10 are highest than the other prepared samples. The bands around 448 and 650 cm^{-1} should be ascribed to the Mn–O and Mn–O–Mn vibrations in octahedral MnO_2 [22, 24–26], which further confirms the successful integration of MnO_2 on the surface of activated carbon.

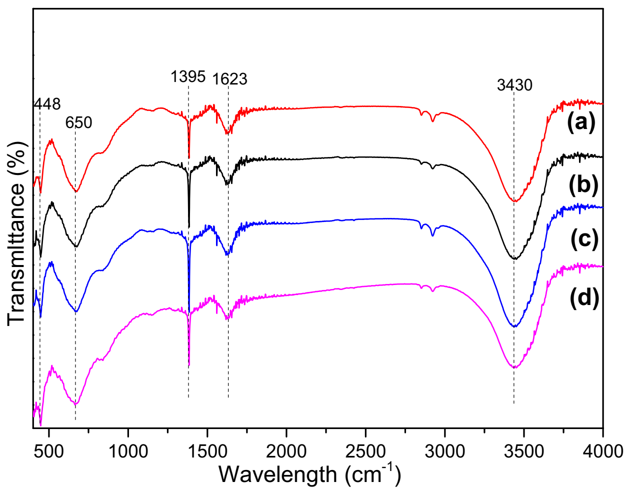

Fig. 6 FTIR spectrum of MnO_2–AC0 (**a**), MnO_2–AC5 (**b**), MnO_2–AC10 (**c**), and MnO_2–AC15 (**d**)

Surface functional groups on the prepared samples were further investigated by XPS analyses. Figure 7 shows the XPS spectrum of the prepared materials (MnO_2–AC0, MnO_2–AC5, MnO_2–AC10, and MnO_2–AC15). The C 1 s pattern of the prepared samples included four peaks with binding energy at around 284.5, 286, 288, and 290 eV. These peaks correspond to graphitizing carbon (C–C), phenolic (C–O), carbonyl carbon (C=O) and transition (π–π*), respectively [27, 28]. The corresponding binding energy and relative content of the samples are listed in Table 2. As shown in Table 2, compared with that in MnO_2–AC0, the content of graphitizing carbon (C–C) in MnO_2–AC5, MnO_2–AC10 decreases, while the content of transition (π–π*) slightly increases. After acid pretreatment of AC, the content of carbonyl carbon (C=O) initially increases with the HNO_3 concentration rising and reaches the maximum value when the HNO_3 concentration is 10 mol/L. The maximum content of carbonyl carbon (C=O) of the as-prepared MnO_2–AC10 was 16.55%. However, when the HNO_3 concentration further increases, the content of carbonyl carbon

Fig. 7 C 1 s patterns of XPS spectra: MnO_2–AC0 (**a**), MnO_2–AC5 (**b**), MnO_2–AC10 (**c**), and MnO_2–AC15 (**d**)

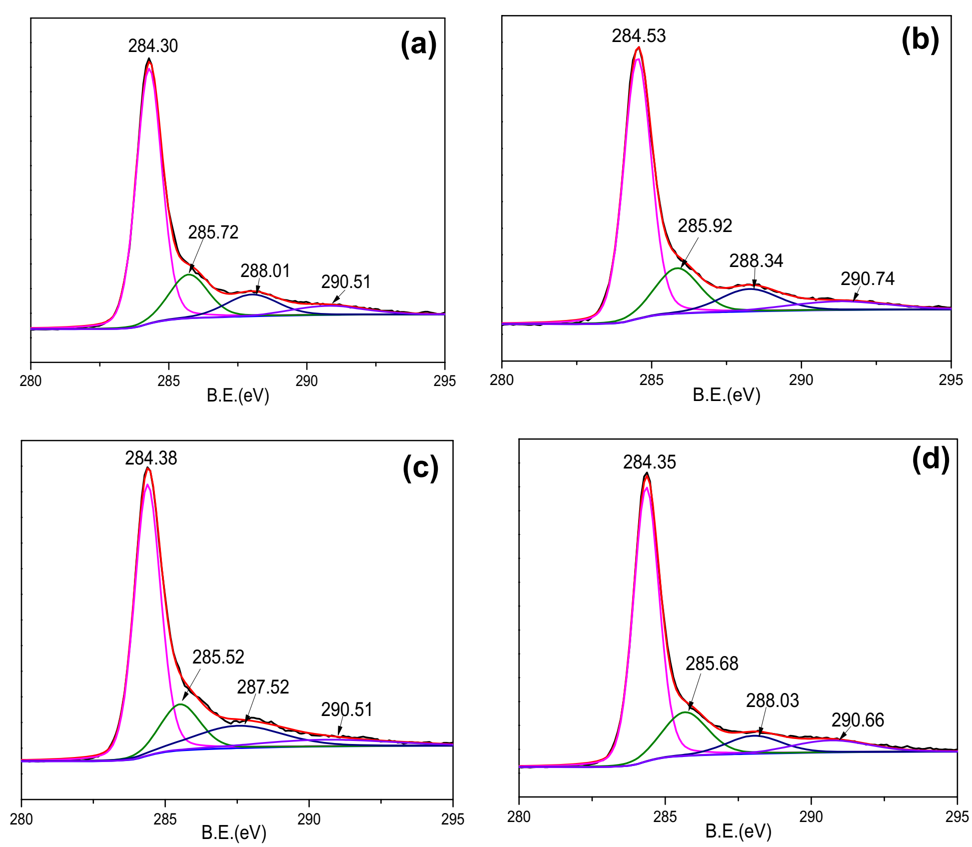

Table 2 Binding energy (BE) and relative content (RC) of C 1 s for MnO_2/AC samples

Sample	MnO_2–AC0		MnO_2–AC5		MnO_2–AC10		MnO_2–AC15	
	BE(eV)	RC(%)	BE(eV)	RC(%)	BE(eV)	RC(%)	BE(eV)	RC(%)
Graphitic carbon	284.3	65.27	284.53	63.10	284.38	60.33	284.35	64.44
Phenolic	285.72	16.93	285.92	17.77	285.52	15.46	285.68	18.08
Carbonyl carbon	288.01	11.28	288.34	11.61	287.52	16.55	288.03	9.15
Transition (π–π*)	290.51	6.52	290.74	7.52	290.51	7.66	290.66	8.33

(C=O) is decreased instead. This result showed a similar change trend with that of FTIR spectra for the prepared samples (shown in Fig. 5).

It is reported that the oxygenated groups of carbonyl carbon (C=O) and transition (π–π*) with the basic nature are more favorable for SO_2 capture [28–31]. Therefore, the change of surface-oxygenated groups, carbonyl carbon (C=O), and transition (π–π*), was responsible for the better SO_2 capture capacity of acid-pretreatment MnO_2/AC composite. Thus, MnO_2–AC10 with the maximum contents of carbonyl carbon (C=O) and transition (π–π*) exhibits the best SO_2 capture capacity among all the prepared materials.

SO_2 capture performance of fresh and regenerated MnO_2-based AC composite

MnO_2–AC10 was chosen to investigate the SO_2 capture performance in low-temperature region due to its superior SO_2 capture performance. The SO_2 capture performance of MnO_2–AC10 is measured by a thermogravimetry (TG) device at various temperatures (50, 100, 150, and 200 °C) for 40 min with a 2 L/min flow gas containing 500 ppm SO_2 in nitrogen, and the results are shown in Fig. 8. From the results shown in Fig. 8, the SO_2 capture performance of MnO_2–AC10 increases with the experimental temperature rising. The prepared MnO_2–AC10 has good SO_2 capture performance with absorbance about 78.3, 59.2, 44.0, and 30.8 mg/g at 200, 150, 100, and 50 °C, respectively.

To investigate the thermal regeneration of MnO_2-based activated carbon composites, the SO_2 capture performance of MnO_2–AC10 sample is studied at 200 and 50 °C with consecutive desulfurization regeneration cycles, and the results are shown in Fig. 9. The SO_2 capture performance of MnO_2–AC10 decreases after thermal regeneration and the decrease trend is more evident at 200 °C. At 50 °C, MnO_2–AC10 has relatively stable regeneration performance with the increase of regeneration cycles, and the SO_2 capture performance of MnO_2–AC10 is about 18 mg/g after two cycles of thermal regeneration. It is reported that SO_2 capture performance of the Mn-modified activated coke decreases after regeneration in N_2 steam, and the desulfurization capacity keeps stable after several cycles of thermal regeneration [28].

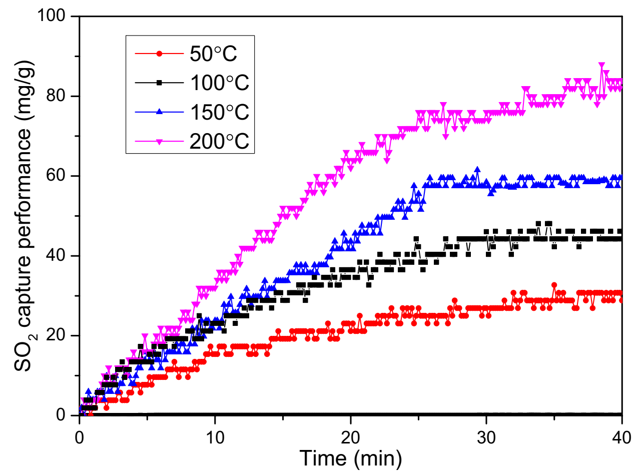

Fig. 8 Temperature dependence of SO_2 capture performance of MnO_2-based activated carbon

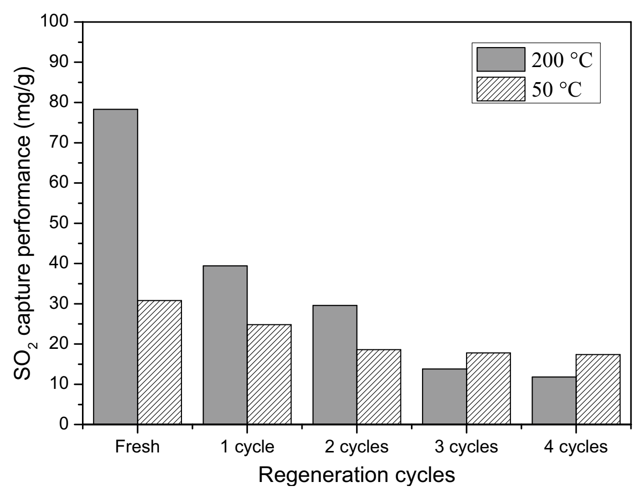

Fig. 9 SO_2 capture performance of MnO_2–AC10 with different regeneration cycles at 50 and 200 °C

Adsorption mechanism

Langmuir and Freundlich models are the most conventional equilibrium adsorption isotherm models to represent the obtained equilibrium data for heterogeneous adsorption on the surface of materials with a chemisorption process.

In this study, the values of the constants for Langmuir and Freundlich models obtained from the experimental equilibrium data of MnO_2-based activated carbon composite (MnO_2–AC10) at a reaction temperature of 100 °C are displayed in Table 3. It is seen that Freundlich model fit the data reasonably well and the value of R-square is as high as 0.998. Freundlich constant (K_f) related to the adsorption capacity of 1.43 was calculated from the intercept of the linear form of the Freundlich model. Freundlich constant (n) related to the adsorption intensity of 2.03 was calculated from the slope of the linear form of Freundlich model. In comparison with the value of Freundlich constant n (1.059) of zeolitic tuff calculated by Al-Harahsheh [32], it is evidenced that the MnO_2-based activated carbon composite exhibits high activity for SO_2 adsorption.

Furthermore, the thermodynamic parameters, such as heat of adsorption (ΔH^0), entropy (ΔS^0) changes, and free energy of the process (ΔG^0) are determined by the following equations (2) and (3):

$$\Delta G^0 = -RT \ln K_f \tag{2}$$

$$\ln K_f = \frac{\Delta S^0}{R} - \frac{\Delta H^0}{RT} \tag{3}$$

where R is the gas constant [8.314 J/(mol K)] and T is the temperature (K), and K_f is the Freundlich constant (L/mg). ΔH^0 and ΔS^0 can be obtained from the slope and intercept of the linear plot of $\ln K_f$ versus 1/T, respectively.

The decrease in negative values of the free energy (ΔG^0) from − 1.11 kJ/mol at 100 °C to − 3.67 kJ/mol at 200 °C suggests that the SO_2 adsorption on MnO_2-based activated carbon composite is a more favorable adsorption process at elevated temperature [32]. The calculated values of ΔH^0 and ΔS^0 are 13.36 kJ/mol and 48.45 J/(mol K), respectively. The positive ΔS^0 and ΔH^0 values indicate that the degrees of freedom increased at the solid–gas interface during the sulfur dioxide capture process [33].

Conclusions

In this study, a series of MnO_2-based AC materials are successfully prepared by deposition method with various concentration of nitric acid treatment to study the influence of surface-oxygenated groups on the SO_2 capture capacity. After preparation, nanoneedle MnO_2 particles are formed and homogeneously dispersed on the AC surface. The SO_2 capture performance of MnO_2-based activated carbon composite initially increases with the HNO_3 concentration rising and reaches the maximum value when the HNO_3 concentration is 10 mol/L because the as-prepared MnO_2–AC10 has the maximum content of surface-oxygenated groups (carbonyl carbon and transition) for capturing SO_2 more favorably. The maximum SO_2-capture capacity of MnO_2–AC10 is 44 mg/g. The SO_2-capture performance of MnO_2–AC10 decreases after regeneration, and the decrease trend is more evident at higher temperature. Furthermore, compared with Langmuir model the experimental data for SO_2 adsorption on MnO_2–AC10 fits the Freundlich model better. The calculated values of ΔH^0 and ΔS^0 were 13.36 kJ/mol and 48.45 J/(mol K), respectively, indicating that the SO_2 adsorption on MnO_2-based activated carbon is a spontaneous process.

Table 3 Isotherm parameters for SO_2 adsorption onto MnO_2–AC10

Model	Constants	R^2
Langmuir	q_m = 117.65 b = 0.001	0.990
Freundlich	K_f = 1.43 n = 2.03	0.998

Acknowledgements This research was supported by the National Natural Science Foundation of China (NSFC) through International (Regional) Cooperation and Exchange Projects (Grant No. 21550110494), Chinese Academy of Sciences President's International Fellowship Initiative (Grant No. 2016VTC068), Guangdong Provincial Science and Technology Plan Projects, P. R. China (Grant No. 2016A050502040).

References

1. Osaka Y, Kito T, Kobayashi N et al (2015) Removal of sulfur dioxide from diesel exhaust gases by using dry desulfurization MnO_2 filter. Sep Purif Technol 150:80–85
2. Lee KT, Bhatia S, Mohamed AR (2005) Preparation and characterization of sorbents prepared from ash (waste material) for sulfur dioxide (SO_2) removal. J Mater Cycles Waste 7(1):16–23
3. Hunsinger H, Andersson S (2014) The potential of SO_2 for reducing corrosion in WtE plants. J Mater Cycles Waste 16(4):657–664
4. Limousy L, Mahzoul H, Brilhac JF et al (2003) A study of the regeneration of fresh and aged SO_x adsorbers under reducing conditions. Appl Catal B: Environ 45(3):169–179
5. Limousy L, Mahzoul H, Brilhac JF et al (2003) SO_2 sorption on fresh and aged SOx traps. Appl Catal B: Environ 42(3):237–249
6. Tikhomirov K, Krocher O, Elsener M et al (2006) Manganese based materials for diesel exhaust SO_2 traps. Appl Catal B: Environ 67(3–4):160–167
7. Liu XC, Osaka Y, Huang HY et al., Development of low-temperature desulfurization performance of a MnO_2/AC composite for a combined SO_2 trap for diesel exhaust. RSC Adv. 2016, *6*, (98), 96367–96375
8. Osaka Y, Kurahara S, Kobayashi N, Hasatani M, Matsuyama A (2015) Study on SO_2-absorption behavior of composite materials for DeSO(x) filter from diesel exhaust. Heat Transfer Eng 36(3):325–332
9. Sohn HY, Han DH (2002) Ca-Mg acetate as dry SO_2 sorbent: III. Sulfation of MgO plus CaO. Aiche J 48(12):2985–2991
10. Zhang D, Ji L, Liu Z et al (2015) Kinetics of thermal regeneration of SO_2-captured V_2O_5/AC. Ind Eng Chem Res 54(38):9289–9295
11. Cantu M, Lopez-Salinas E, Valente JS (2005) SO_x removal by calcined MgAIFe hydrotalcite-like materials: Effect of the chemical

composition and the cerium incorporation method. Environ Sci Technol 39(24):9715–9720
12. Rubio B, Izquierdo MT (2010) Coal fly ash based carbons for SO_2 removal from flue gases. Waste Manage 30(7):1341–1347
13. Tseng HH, Wey MY (2004) Study of SO_2 adsorption and thermal regeneration over activated carbon-supported copper oxide catalysts. Carbon 42(11):2269–2278
14. Liu X, Osaka Y, Huang H et al (2016) Development of high-performance SO_2 trap materials in the low-temperature region for diesel exhaust emission control. Sep Purif Technol 162:127–133
15. Liu X, Osaka Y, Huang H et al (2017) Development of compact MnO_2 filter for removal of SO_2 from diesel vehicle emission. RSC Adv 7:18500–18507
16. Liu Y, Qu Y, Guo J et al (2015) Thermal regeneration of manganese supported on activated carbons treated by HNO_3 for desulfurization. Energy Fuels 29(3):1931–1940
17. Zhang G, Li Z, Zheng H et al (2015) Influence of the surface oxygenated groups of activated carbon on preparation of a nano Cu/AC catalyst and heterogeneous catalysis in the oxidative carbonylation of methanol. Appl Catal B: Environ 179:95–105
18. Xu J, Zhao J, Xu J et al (2014) Influence of surface chemistry of activated carbon on the activity of gold/activated carbon catalyst in acetylene hydrochlorination. Ind Eng Chem Res 53(37):14272–14281
19. Alegre C, Gálvez ME, Baquedano E et al (2013) Oxygen-functionalized highly mesoporous carbon xerogel based catalysts for direct methanol fuel cell anodes. J Phys Chem C 117(25):13045–13058
20. Rodrigues EG, Pereira MFR, Chen X et al (2011) Influence of activated carbon surface chemistry on the activity of Au/AC catalysts in glycerol oxidation. J Catal 281(1):119–127
21. Aguilar C, García R, Soto-Garrido G et al (2003) Catalytic wet air oxidation of aqueous ammonia with activated carbon. Appl Catal B: Environ 46(2):229–237
22. Yuan A, Zhang Q (2006) A novel hybrid manganese dioxide/activated carbon supercapacitor using lithium hydroxide electrolyte. Electrochem Commun 8(7):1173–1178
23. Xia Y, Meng L, Jiang Y et al; Zhao M (2015) Facile preparation of MnO_2 functionalized baker's yeast composites and their adsorption mechanism for Cadmium. Chem Eng J 259:927–935
24. Lu L, Tian H, He J et al., Graphene-MnO_2 Hybrid nanostructure as a new catalyst for formaldehyde oxidation. J Phys Chem C 2016, *120*, (41), 23660–23668
25. Xie X, Gao L (2007) Characterization of a manganese dioxide/carbon nanotube composite fabricated using an in situ coating method. Carbon 45(12):2365–2373
26. Chu HY, Lai QY, Wang L et al (2010) Preparation of MnO_2/WMNT composite and MnO_2/AB composite by redox deposition method and its comparative study as supercapacitive materials. Ionics 16(3):233–238
27. Guo JX, Fan L, Peng JF et al (2014) Desulfurization activity of metal oxides blended into walnut shell based activated carbons. J Chem Technol Biotechnol 89(10):1565–1575
28. Yang L, Jiang X, Yang ZS et al (2015) Effect of $MnSO_4$ on the removal of SO_2 by manganese-modified activated coke. Ind Eng Chem Res 54(5):1689–1696
29. Fan L, Chen J, Guo J et al (2013) Influence of manganese, iron and pyrolusite blending on the physiochemical properties and desulfurization activities of activated carbons from walnut shell. J Anal Appl Pyrol 104:353–360
30. Shangguan J, Li CH, Miao MQ et al (2008) Surface characterization and SO_2 removal activity of activated semi-coke with heat treatment. New Carbon Mater 23(1):37–43
31. Zuo Y, Yi H, Tang X, Zhao S, Zhang B, Wang Z, Gao F (2015) Study on active coke-based adsorbents for SO_2 removal in flue gas. J Chem Technol Biotechnol 90(10):1876–1885
32. Al-Harahsheh M, Shawabkeh R, Batiha M et al (2014) Sulfur dioxide removal using natural zeolitic tuff. Fuel Process Technol 126(0):249–258
33. Gupta VK, Ali I, Suhas et al (2003) Equilibrium uptake and sorption dynamics for the removal of a basic dye (basic red) using low-cost adsorbents. J Colloid Interface Sci 265(2):257–264